Experimental results of a Differential Optic-Flow System

Richard Kathage and Jonghyuk Kim
Department of Engineering
The Australian National University, Australia
{richard.kathage, jonghyuk.kim}@anu.edu.au

Abstract

Visual odometry through the use of optical-flow has drawn significant interest within the robotics and navigation community. Its implementation provides a self-contained system which is well aligned to the biological strategy employed by flying insects. There have been several progressions in using optic-flow measurement combined with other sensors like GPS or ultrasonics to resolve depth and velocity information. Although the results are promising, they are not fully self-contained and rely on additional sensors for external information. As a self-contained system, a differential optic-flow system had been developed which addresses this issue. This paper will provide experimental results of the performance of a differential optic flow system in both an indoor and outdoor environment. From these experiments it was found that the system performed better within the outdoor setting than the indoor setting due to the rich textures and good lighting conditions found within an outdoor environment.

1 Introduction

Optical flow is defined as the speed of motion of an image. It is an visual motion phenomenon experienced by humans,animals, and some insects. Within the concept of Optical flow height and velocity are proportional to one other. This motion can used to infer information about the state of the observer relative to the visual environment, such as height and velocity. Odometry can thus be determined from accumulated velocity measurements [Barron and Srinivasan, 2006].

Traditional odometry sensor systems in mobile/ground vehicles generally include the use of wheel encoders and/or steering angle sensors. Although quite successful, they are susceptible to errors like wheel slippage and more importantly they require physical intervention of the system to get the sensor information.

Odometry measurement through a visual implementation (such as optical flow) can provide a self-contained system which addresses the issues associated with traditional odometry systems. Recent advances in low-cost cameras and digital signal processing have made it possible to embed the visual odometry devices on single chip. This technology has been utilised by several manufacturers in development a chip that is dedicated to measuring displacement through optic flow (i.e optical mouse sensors). The accumulated optic-flow however is not directly the Euclidian displacement due to the unknown depth to the surface or the unknown speed of the camera. If the additional kinematic information is available, such as the height of the camera, it can be used to measure the ground displacement as in [Brenner and Smeets, 2003] and odometry estimation [Palacin *et al.*, 2006]. Without such information, it can still be used to avoid obstacles or reactive guidance [Lim *et al.*, 2006], or even for pure topological odometry within an urban road network [Milford and Wyeth, 2008].

In aerial robotics, the use of a visual odometry system becomes more attractive given the payload-limitations. [Jufferey and Floreano, 2006] showed the embedded optic-flow sensor could be used for robotic aerial vehicles. [Griffiths, 2006] has developed an optic flow sensor using an optical mouse chip. The system was then successfully used in conjunction with GPS velocity measurements to determine the height and displacement of a UAV. Similar researchers [Danko *et al.*, 2005] have used mouse optic flow sensors with ultrasonic sensors to land a model helicopter autonomously.

Although successful, the optical-flow sensor has however had to be used with the aid of velocity or height measurement from another sensor such as GPS or ultrasonic. To achieve a fully self-contained system, a differential optic-flow system was developed in the previous work [Kim and Brambley, 2007], which showed that the system could be used to determine both height and velocity in indoor conditions.

In this paper, a more in-depth analysis involving ex-

tensive experiments have been conducted to assess the system in various operating conditions. The outdoor environment is more challenging than the controlled indoor condition due to the different optical and lighting conditions which are not originally intended for optical mouse chips. The terrain beneath the vehicle is not guaranteed to be flat, nor comprise of homogeneous textures. Furthermore, the level of light enveloping the surface is not guaranteed to be of any specific wavelength or intensity. Therefore to validate the system developed in this environments, several experiments have been conducted on a 6-DOF ABB manipulator arm and a land vehicle with varying optic-flow sampling rates and trajectories.

This paper is structured as follows: Section 2 describes the raw optic-flows with a method to compensate the body-induced rotational motion and to compute the height above ground. Section 3 presents the considerations to achieve the best performance in terms of operating height, sampling rate and vehicle speed. Section 4 will provide experimental setups and results on an indoor robot manipulator and an car platform with conclusions in Section 5.

2 Optic-Flows in 6DOF Platforms

The optic flow sensors were designed for use inside a standard desktop mouse. In this environment the lighting is precisely controlled and the reference surface has specific textural properties. When fitted to a moving 6DoF vehicle however, the environmental conditions are no longer ideal. That is in most instances, the optical axis of the camera will not be perpendicular to the terrain beneath the vehicle. This is due to the rotational motion and orientation of the vehicle and the gradient of surrounding terrain. In addition the intensity and wavelength of the light will not be controllable.

The processing of the optic-flow data to get the height and ground velocity information is outlined in Figure 1 and as followings:

- Rotational Motion Compensation: The raw optic-flow measurements need to be processed to eliminate the effects of platform's rotational motion using the angular velocity measured from inertial sensors.
- Range to surface computation: By using the vertically separated two optic-flows, the range to the terrain surface can be computed as well as the ground velocity.
- Height above ground: The range to the surface can then be converted into height above ground by using the orientation information from the inertial systems.

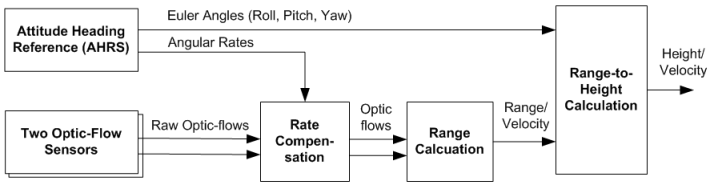

Figure 1: A diagram for processing raw optic-flow data and inertial data to compute the height-above-ground and velocity.

2.1 Raw Optic-flow Measurement

The optic-flows measured in a sensor are accumulated pixel counts $(n_x,\ n_y)$ over sampling time Δt. These need to be converted to angular increments in radians $(\Delta\theta_x,\ \Delta\theta_y)$ using camera parameters:

$$\Delta\theta_x = \left(\frac{\alpha}{n_p}\right) n_x, \quad \Delta\theta_y = \left(\frac{\alpha}{n_p}\right) n_y \tag{1}$$

with α/n_p is a conversion factor using the field-of-view (in radians) and the principle pixel dimension (in pixels) within the camera, respectively.

The total optic-flow in radians is also related to the vehicle motion as a ratio of the linear distance travelled $(v_g \Delta t)$ and height-above-ground (h). That is, $\Delta\theta = (v_g \Delta t)/h$. This relationship will be used in the following discussions to compute the height-above-ground from the dual optic-flow measurements.

2.2 Rotational Motion Compensation

Vehicle rotation rates $(\omega_x, \omega_x, \omega_z)$ and optic flows are highly coupled since the camera is rigidly mounted onto the vehicle body. In this work the camera of the optic flow sensor is installed pointing downward which is defined as the z-axis, while the x-axis of the frame being aligned with the forward direction of the vehicle and y-axis completing the right-handed. Any rotational motion about the x or y axes will manifest as optic flow. This is true even if the vehicle is not translating relative to the navigation frame. As the coordinate systems of the flow sensors are aligned with the body frame, a rotation about the x axis will appear as a change in the optic flow of the y axis, and vice versa.

This rotational motion can be effectively compensated for using the angular velocity $(\omega_x, \omega_x, \omega_z)$ measured from the inertial sensor suite. That is from the Figure 2 the angular velocity vector can be converted into the equivalent optical-flow rate vector in the image plane by performing a vector cross-product with the focal length vector.

$$\begin{bmatrix} \dot{\theta}_x \\ \dot{\theta}_y \\ \dot{\theta}_z \end{bmatrix} = \begin{bmatrix} \omega_x \\ \omega_y \\ \omega_z \end{bmatrix} \otimes \begin{bmatrix} 0 \\ 0 \\ f \end{bmatrix} = \begin{bmatrix} \omega_y f \\ -\omega_x f \\ 0 \end{bmatrix} \tag{2}$$

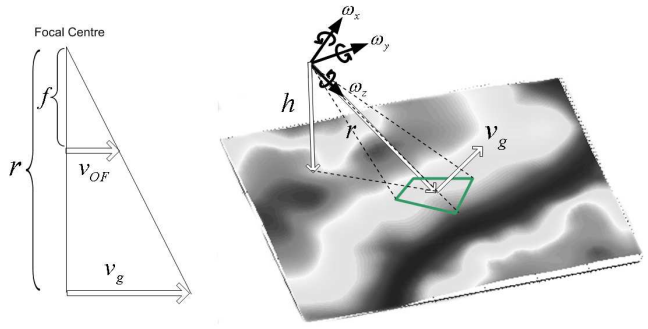

Figure 2: Sensing geometry in a 6DoF platform. The image motion and ground velocity (left) and the geometry for the height calculation from the range information in near-flat terrains.

These terms are then subtracted from the raw optic flow measurements. Note that the rotation motion along the z-axis of the body frame would not affect this correction. This is because that the optic flow around the centre of the image will be averaged out resulting in a zero-flow.

2.3 Range-to-Surface and Ground Velocity

From a single optic-flow measurement, the ground speed and range-to-surface can not be computed separately, giving only the ratio of them. This is overcome in this work by placing a second optic flow sensor with the same orientation, but displaced by a distance L, along the z-axis of the body frame. By using the relationship in the single sensor case and the length constraint to the two optic-flows yields

$$r_1 = \frac{v_g \Delta t}{\Delta\theta_1}, \quad r_2 = \frac{v_g \Delta t}{\Delta\theta_2}, \quad L = r_2 - r_1. \tag{3}$$

Applying some algebraic manipulations gives

$$r_1 = L\left(\frac{\Delta\theta_2}{\Delta\theta_1 - \Delta\theta_2}\right), \tag{4}$$

and subsequently the ground speed being

$$v_g = L\left(\frac{\Delta\theta_2}{\Delta\theta_1 - \Delta\theta_2}\right)\frac{\theta_1}{\Delta t}. \tag{5}$$

2.4 Height above ground

From the Figure 2, the height above the ground h can be computed using the Euler angles, roll (ϕ), pitch (θ) and yaw ψ, and the computed range-to-surface r in previous section. The coordinate transformation matrix between a body-frame referenced vector and a ground-frame referenced vector becomes,

$$C_b^n = \begin{bmatrix} C_\theta C_\psi & -C_\phi S_\psi + S_\phi S_\theta C_\psi & S_\phi S_\psi + C_\phi S_\theta C_\psi \\ C_\theta S_\psi & C_\phi C_\psi + S_\phi S_\theta C_\psi & -S_\phi C_\psi + C_\phi S_\theta S_\psi \\ -S_\theta & S_\phi C_\theta & C_\phi C_\theta \end{bmatrix}. \tag{6}$$

Assuming the terrain undulation is not significant, the vertical height can be approximated to the projection of the range vector to the vertical direction. That is

$$h = (r\hat{\mathbf{k}}) \cdot \hat{\mathbf{K}} \tag{7}$$

where $\hat{\mathbf{k}}$ is the unit vector of the z-axis in the body-frame and $\hat{\mathbf{K}}$ is the unit vector in the navigational frame which is equivalent to $C_b^n\hat{\mathbf{k}}$, thus giving

$$\begin{aligned} h &= r\hat{\mathbf{k}} \cdot (C_b^n \hat{\mathbf{k}}) = \begin{bmatrix} 0 \\ 0 \\ r \end{bmatrix} \cdot \begin{bmatrix} S_\phi S_\psi + C_\phi S_\theta C_\psi \\ -S_\phi C_\psi + C_\phi S_\theta S_\psi \\ C_\phi C_\theta \end{bmatrix} \\ &= r\cos\phi\cos\theta. \end{aligned} \tag{8}$$

3 Constraints in using Optic-flows

The performance of the differential optic-flow system depends on various operating conditions, including height, vehicle speed and sampling rate.

Optical flow is proportional to the height-above-ground. Therefore increasing the distance between two optical sensors will produce larger motion values for the sensor closest to the ground, and smaller motion values for the sensor furthest from the ground. This then allows for a greater pixel difference between the two motion values, allowing the height-above-ground to be determined with greater precision [Kim and Brambley, 2007]. The sensor displacement therefore should be maximized where possible, which is however fairly limited in most physical systems.

Instead, the lower sampling rate of the optical chips can also be used to increase the pixel difference between the two optical flow sensors. The internal sampling rate of an optical mouse sensor is fixed at a predefined rate and cannot be modified. The internal sampling rate is equivalent to the rate at which the sensors camera acquires images which is 1500 frame-per-second in the system used. Although the sampling rate of the sensor cannot be directly modified, it can be indirectly modified by changing the rate at which the raw optic flow data is accumulated.

The optic flow data values within the optic chips register are accumulated until either the register overflows (when motion value is greater than 127 pixels), or the host micro-controller reads the register. Therefore the sampling rate can be effectively controlled by altering the amount of motion which is accumulated within the register.

It should be noted that the pixel difference can also be increased by the increasing the speed of the platform. However with the lower sampling rate, it will be more susceptible to the overflow condition within the motion registers and thus needs a higher sampling rate. This means the low-frequency sampling scheme is limited to

low velocity at small heights and high velocity at larger heights. This will be vice versa for larger frequency rates. Based on these considerations the sampling rate should be dynamic and match the operating conditions for the best performance.

4 Experimental Results

To verify the performance in various conditions, a prototype has been implemented and tested on a robotic arm manipulator and a car.

4.1 Sensor Systems

Two Agilent adns-3080 mouse chips were chosen for the optical sensors as shown in Figure 3. It is a non-mechanical optical tracking sensor that is commonly found in computer mice. It measures changes in position by way of determining the direction and magnitude of motion from sequential surface images. The images are nominally acquired at a rate of 1500 frames-per-second which are then analysed by an in-built image-processing algorithm. Specific surface features on the image plane are identified and have their positions tracked with each frame. The collective motion of surface features are assigned two displacement values (i.e X and Y) describing their overall motion across the image plane. The displacement values are then given in terms of pixel counts. Two button lens with a small field of view (17°) and focal length of $25mm$ were used to provide clear images so that the chip can track features reliably at a distance. The inertial measurement unit used was 3DM-GX1 manufactured by Micro-strain as shown in Figure 3, which is low-cost and delivers rotational rates and Euler angles. A Gumstix single board computer was used to interface the sensors and ground monitoring system through a wireless connection.

Figure 3: Agilent optical-mouse chip (left) and MicroStrain 3DMG inertial measurement unit (right) used for experiment.

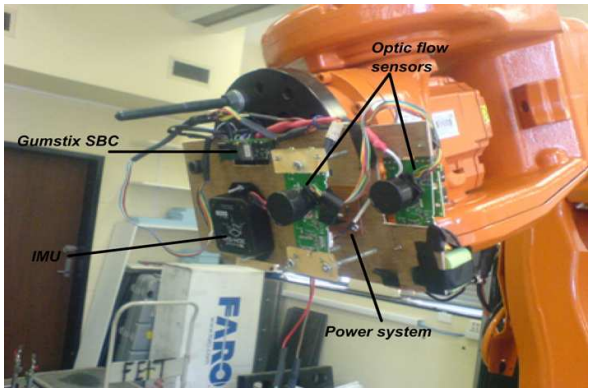

Figure 4: A differential Optic-flow system installed on the end effector of an ABB manipulator

4.2 Robot Manipulator

The system was attached to an ABB arm manipulator using a custom designed mechanical mount. Two paths were then programmed into the ABB arm manipulator with descending and ascending trajectories. The surface was illuminated with a $45W$ lamp placed 45° at the surface. A $10Hz$ sampling rate with 5.5cm displacement between two optic flow sensors was used.

Figure 5: A differential Optic-flow system installed on a car bike rack

4.3 Outdoor Experiment

The purpose of this experiment was to test the performance of the system in a realistic outdoor environment which has different texture and light level which will not be controlled as easily compared to the indoor experiment. The system was attached to the back of a car using a bike rake as shown in the Figure 5. The two optic flow sensors were orientated such that the x-axis of

the sensors were orientated parallel to the forward vehicles direction. The car was then driven through an open grass field of $117m$ with an average speed of $5km/hr$ as shown in Figure 6. The experiment was conducted on a sunny day with no cloud cover.

4.4 Manipulator Result

For the test on the robot arm manipulator, the raw measurements and low-pass filtered height are shown in Figures 7 and 8. As the robot manipulator descends with horizontal motion, two optical sensors pick up the increased flow measurements with a slight offset due to the separation of two sensors. Between descending and ascending motion, the manipulator stopped temporarily resulting in zero flow measurements. The height above ground was computed from the raw measurements and then filtered using a low-filter to reduce the noise. At some time intervals, the computed height is comparable to the truth from the manipulator trajectory. However, it can be seen that there exists inconsistencies mostly due to the lack of features. This was confirmed from the number of features tacked from the optical sensor which was below the minimum recommended number.

4.5 Outdoor Result

Figures 9 and 10 show the recorded raw data and low-pass filtered data for the forward movement. The raw data shows both sensors attaining similar values with the first sensor (sensor 1 in the plot) with higher values as expected, while showing significant noise in the second sensor due to the lower installation. Significant noise present mostly stemming from the non-rigid installation of the second sensor coupled with vibration in the bike rack. The filtered data shows the offset between two sensors more clearly. The initial and final drops in the optic measurement were due to the low speed during acceleration and deceleration of the car. Figure 11 shows the height-above-grounds computed from two optic flows with additional low-pass filtering. The three drive tests showed repeatable and good performance showing $\pm 20cm$ errors from the actual height of $150cm$. The reasons for this better performance in outdoor environment was mostly due to the rich textures and constant light intensity of the sun over the operating field. This confirmed from the high number of features tracked from the optical chips. The number dropped frequently due to the shadows from trees but it showed significantly better than expected and generally better than that of the experiments conducted in doors.It was found however that certain outdoor environments such as roads or monotonous car park places showed significantly low level of features due to the poor textures.

Figure 6: Vehicle path measured by GPS during the car experiment.

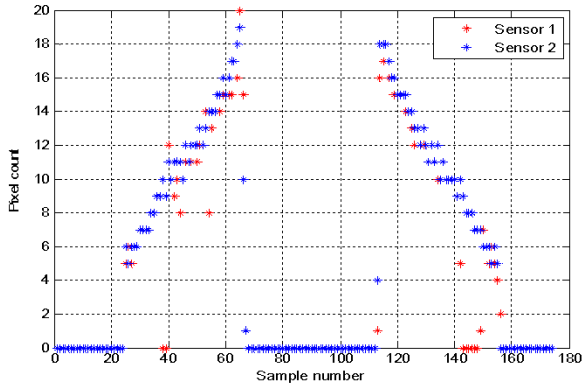

Figure 7: The raw optic-flow measurements showing increased optic flows as the manipulator approaching ground. The zero readings in the middle of the plot are when the manipulator stopped,resulting in zero optic flow

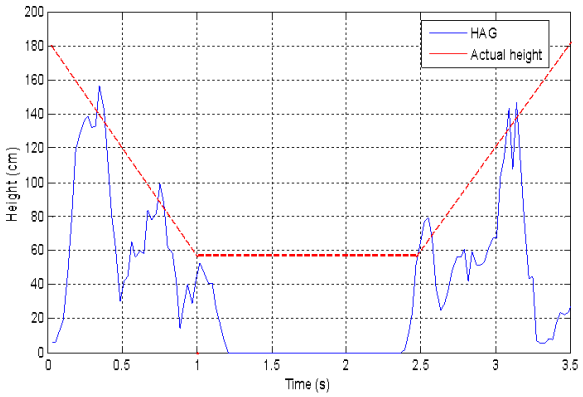

Figure 8: The height computed from the differential optic-flows during the experiment

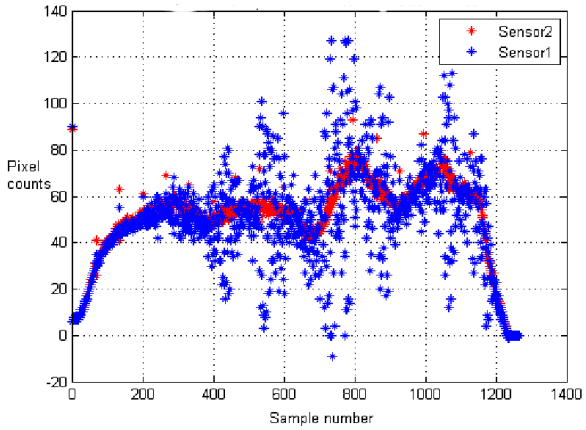

Figure 9: Raw optic-flow measurements in pixel counts from two sensors

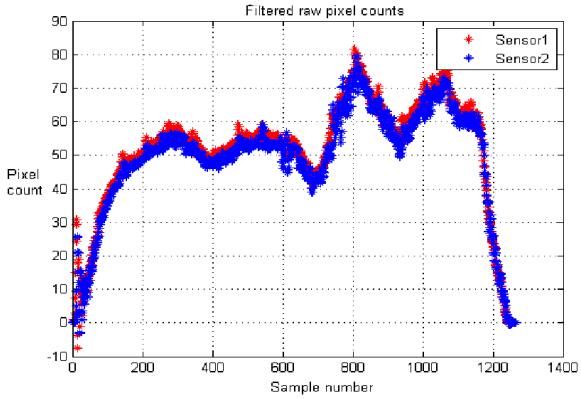

Figure 10: Low-pass filtered flow measurements in pixel counts showing differences between two sensors

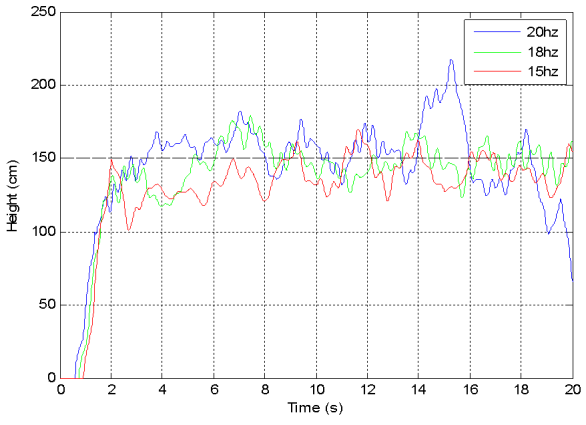

Figure 11: The height computed from the differential optic-flow system with three driving tests

5 Conclusions

This paper presented outdoor experimental results to show the feasibility of using optical-mouse chips as a self-contained navigational sensor. The differential operation of the optic-flow provided the capability of depth resolution to the terrain without relying on external velocity sensors like GPS. The field experiments showed that within a range of outdoor environments, it can provide an accurate and cost-effective visual odometry solution. The high sensitivity of the system to sensor noises can be further relieved by integrating the system with other navigational systems like GPS/INS system.

References

[Barron and Srinivasan, 2006] A. Barron and M.V. Srinivasan. Visual regulation of ground speed and headwind compensation in freely fying honey bees. 209, 2006.

[Brenner and Smeets, 2003] E. Brenner and J.B.J. Smeets. Fast corrections of movements with a computer mouse. *Spatial Vision*, 16:365–376, 2003.

[Danko *et al.*, 2005] T.W. Danko, A. Kellas, and P.Y. Oh. Robotic rotorcraft and perch-and-stare: sensing landing zones and handling obscurants. In *IEEE International Conference on Robotics and Automation*, 2005.

[Griffiths, 2006] S.R. Griffiths. Remote terrain navigation for unmanned air vehicles. *Master Thesis, Brigham Young University*, 2006.

[Jufferey and Floreano, 2006] J.C. Jufferey and D.F Floreano. Fly-inspired visual steering of an ultralight indoor aircraft. *IEEE Transactions on Robotics*, 22(1):137–146, 2006.

[Kim and Brambley, 2007] J. Kim and G. Brambley. Dual Optic-flow Integrated Navigation for Small-scale Flying Robots. In *Australasian Conference on Robotics and Automation*, 2007.

[Lim *et al.*, 2006] J. Lim, C. McCarthy, D. Shaw, L. Cole, and N. Barnes. Insect Inspired Robots. In *Australasian Conference on Robotics and Automation*, 2006.

[Milford and Wyeth, 2008] M.J. Milford and G.F. Wyeth. Single camera vision-only SLAM on a suburban road network. In *IEEE International Conference on Robotics and Automation*, pages 3684–3689, 19-23 May 2008.

[Palacin *et al.*, 2006] J. Palacin, I. Valga non, and R. Pernion. The optical mouse for indoor mobile robot odometry measurement. *Sensors and Actuators*, 126:141–147, 2006.